Comprehensive quantitative characterization of the human term amnion proteome

Eva Avilla-Royo [a,b]**, Katharina Gegenschatz-Schmid** [a]**, Jonas Grossmann** [c,e]**, Tobias Kockmann** [c]**, Roland Zimmermann** [a,f]**, Jess Gerrit Snedeker** [b,d]**, Nicole Ochsenbein-Kölble** [a,f] **and Martin Ehrbar** [a,g]*

a - **Department of Obstetrics,** *University and University Hospital of Zurich, 8091 Zurich, Switzerland*

b - **Institute for Biomechanics,** *Swiss Federal Institute of Technology, 8093 Zurich, Switzerland*

c - **Functional Genomics Center,** *University of Zurich and ETH Zurich, 8057 Zurich, Switzerland*

d - **Department of Orthopedics,** *Balgrist University Hospital, University of Zurich, 8008 Zurich, Switzerland*

e - **SIB Swiss Institute of Bioinformatics,** *1015 792 Lausanne, Switzerland*

f - **The Zurich Center for Fetal Diagnosis and Therapy,** *8032 Zurich, Switzerland*

g - **University of Zurich,** *8006 Zurich, Switzerland*

Correspondence to Martin Ehrbar: Schmelzbergstrasse 12, PATH G48, 8091 Zurich, Switzerland.
martin.ehrbar@usz.ch (M. Ehrbar)
https://doi.org/10.1016/j.mbplus.2021.100084

Abstract

The loss of fetal membrane (FM) integrity and function at an early time point during pregnancy can have devastating consequences for the fetus and the newborn. However, biomaterials for preventive sealing and healing of FMs are currently non-existing, which can be partly attributed to the current fragmentary knowledge of FM biology. Despite recent advances in proteomics analysis, a robust and comprehensive description of the amnion proteome is currently lacking. Here, by an optimized protein sample preparation and offline fractionation before liquid chromatography coupled to mass spectrometry (LC-MS) analysis, we present a characterization of the healthy human term amnion proteome, which covers more than 40% of the previously reported transcripts in similar RNA sequencing datasets and, with more than 5000 identifications, greatly outnumbers previous reports. Together, beyond providing a basis for the study of compromised and preterm ruptured FMs, this comprehensive human amnion proteome is a stepping-stone for the development of novel healing-inducing biomaterials. The proteomic dataset has been deposited in the ProteomeXchange Consortium with the identifier PXD019410.

Introduction

The fetal membranes (FMs), namely the amnion and the chorion, are extraembryonic tissues that surround the fetus throughout pregnancy in all vertebrates [1]. Their main functions include the retention of the amniotic fluid (AF), the exchange of nutrients, gas and waste products between the AF and the uterus [2], and the protection of the fetus against infections and physical impacts [3]. In a healthy pregnancy, the FMs surround a tightly closed cavity and maintain their integrity throughout gestation (Fig. 1). At term, they rupture in preparation for delivery, a process that was previously thought to be mainly mechanical. More recent publications have associated the factors that participate in extracellular matrix (ECM) remodeling with the aging and failure of the FMs [4], and it is believed that degradation of the collagen-rich ECM is one of the key factors that leads to FM rupture [5].
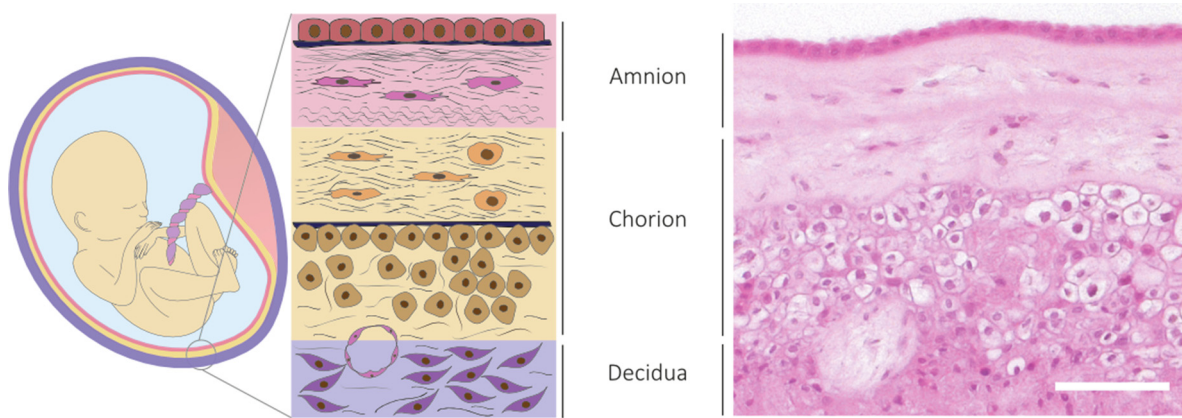
Fig. 1. Structure of the fetal membranes. The fetal membranes are composed of the amnion and the chorion. The decidua is the inner lining layer of the uterus. Right: Hematoxylin/Eosin staining of the FMs, where the different layers are appreciated. Scale bar is 100 μm.

Failures of the FMs have been reported to be the main identifiable cause of preterm births [6] (before 37 weeks of gestation) which can result in mild to severe morbidities or even the mortality of newborns [7,8]. Spontaneous preterm premature rupture of the fetal membranes (sPPROM) has been reported to affect 4–5% of all pregnancies in high income countries, and is expected to have a higher incidence in low income countries [5]. sPPROM is thought to be a multifactorial problem of which several mechanisms, including infection, stress and immunologic processes are thought to be initiators [9]. With the advance of fetal diagnosis and the increase of minimally invasive prenatal surgical interventions, a new type of PPROM, called iatrogenic PPROM (iPPROM), has appeared. iPPROM remains the main complication after such interventions and occurs in about 30–50 % of the cases after an intervention in the amniotic cavity [10–13]. This high incidence of iPPROM has been attributed to several factors [13,14] such as the lack of spontaneous healing of the FMs which, although not fully understood yet, is believed to partially relate to the poor vascularization of the FMs [15,16]. Despite great need to carry on a pregnancy until 37–40 weeks of gestation, there are currently neither methods nor biomaterials available to restore FM integrity [17].

The initiation of FM rupture was long considered to result from a mechanical failure of the FMs [18,19], and for this reason several studies have focused on correlating the mechanical properties of the FMs with the composition and structure of their ECM [20,21]. However, in the past decades it became clear that the ECM plays essential roles in directing an array of cellular functions such as cell differentiation, proliferation, polarity, survival and migration [22]. Both by the presentation of cell adhesion and signaling sites and by the mechanical properties of the matrix, the ECM mediates and regulates processes such as morphogenesis, tissue homeostasis and wound healing [23,24]. Factors that steer ECM remodeling and turnover, such as matrix metalloproteinases (MMPs) and their inhibitors (TIMPs) [5,25–28] could be involved in the maturation and sterile inflammation of the FMs, eventually leading to their premature rupture [4,5]. Additionally, several studies indicated that the FMs may have the ability to heal and regenerate through the recruitment of resident FM cells, when treated with biomaterials and appropriate signaling molecules [29–33]. For example, the use of collagen type I was shown to increase closure rate in a mouse model [33], and the migration of cells into implanted Matrigel was observed in rabbits [34]. Hence, the identification of novel signals could be employed for the design of biomaterials with a healing-promoting function that could prevent iPPROM.

The protein composition of the human amnion has been characterized using methods such as western blot and protein microarrays [35,36]. Although highly specific, these methods are limited by their low-medium throughput and the low yield of identifications. Similarly, immunohistochemistry (IHC) has been important in understanding the major composition of the FMs [1,37] but it is limited by antibody cross-reactivity and lack of universal protocols. Furthermore, these methods make quantification of protein abundance difficult. First proteomic studies on the amnion were based on 2-dimensional gel electrophoresis followed by peptide mass fingerprint (PMF) analysis [38–40], or used isobaric tagging for relative quantification (iTRAQ) and focused solely on the soluble fraction of the amnion proteome [36]. In the past decade, mass spectrometry-based proteomics emerged as the method of choice to obtain an unbiased and untargeted proteome of various tissues [41] and was the method employed when drafting the human proteome in 2014 [42]. However, a thorough and methodically up-to-date description of the human amnion proteome is currently inexistent.

In this study, we used liquid chromatography coupled to mass spectrometry (LC-MS) to characterize the proteome of the healthy human term amnion. First, we established a method for the preparation of samples that enabled a reliable and unbiased proteomic evaluation. Then, by combining the optimized sample preparation procedure, the offline peptide fractionation (using 9 fractions) and LC-MS/MS analysis, we identified more than 5000 proteins. An analysis of this vast proteome enabled the identification of 285 ECM proteins, a knowledge that can be used to understand the biology of FM integrity. Furthermore, we identified novel proteins that are related to how FM cells interact with their surrounding ECM, among which MMPs, TIMPs, growth factors and their receptors. This optimized and global unbiased proteomic approach is an addition to the current fragmented knowledge on human FMs, as it provides a quantitative characterization of the human amnion composition. Furthermore, it opens the door to the study of preterm or punctured FMs and their inability to heal.

Materials and methods

Sample collection

Fetal membranes were collected immediately after delivery from healthy donors who had an uncomplicated pregnancy and underwent elective cesarean section with written consent, following the decision from the Ethical Committee of the District of Zurich (study Stv07/2007). The FMs were verified to be negative for HIV and hepatitis B, signs of infection and chromosomal abnormalities. The amnion and the chorion were cut about 5 cm from the placental disc and outside the zone of altered morphology. They were then separated by blunt dissection and the amnion was rinsed three times with phosphate buffered saline solution (PBS) containing protease inhibitors (cOmplete™ protease inhibitors cocktail, Roche) at 37 °C. The amnion was then snap-frozen in liquid nitrogen and stored at −80 °C until further processing. Then, it was ground under liquid nitrogen into a fine powder.

Protein extraction, digestion, and peptide purification

Two sample preparation methods that have been reported suitable for the study of proteins that are hard to solubilize were used. The urea-based sample preparation includes urea-based extraction and in-solution digestion. The filter-aided sample preparation (FASP) includes an SDS-based extraction and in-filter digestion.

Urea-based sample preparation. 100 mg of pulverized tissue were incubated with 500 µl urea buffer (UA; 8 M urea in 0.1 M Tris buffer solution pH 8.2 (TBS) supplemented with protease inhibitors (cOmplete™ protease inhibitors cocktail, Roche)) for 30 min on ice and centrifuged at 16'000 g, 4 °C for 20 min. Samples were then diluted with TBS to 6 M urea and protein concentration was measured with a NanoDrop spectrophotometer at an absorbance of 280 nm. The corresponding volume to 20 µg of extracted protein was prepared as follows: Disulfide bonds were reduced with the addition of dithiothreitol (DTT) to a final concentration of 5 mM and incubated for 30 min at room temperature (RT). Then, free cysteines were alkylated by the addition of iodoacetamide (IAA) to a final concentration of 50 mM and LysC (Lysyl Endopeptidase Mass Spectrometry Grade, Wako Pure Chemical Corporation) was added in a 1:20 protease to protein ratio (w/w) to pre-digest the proteins for 1 h at RT in the dark. After dilution to 1 M urea with TBS, sequencing grade trypsin (Promega) was added in a 1:50 protease to protein ratio (w/w) and incubated overnight in the dark at RT. Peptides were centrifuged for 20 min at 16'000 g and then acidified to a final concentration of 0.5% trifluoroacetic acid (TFA, Thermo Fisher Scientific).

Filter-aided sample preparation (FASP). 100 mg of pulverized tissue were incubated with 500 µl sodium dodecyl sulfate (SDS) lysis buffer (4% SDS (w/v) in TBS containing 0.1 M DTT and protease inhibitors (cOmplete™ protease inhibitors cocktail, Roche)) for 5 min at 95 °C and centrifuged at 16'000 g for 10 min at RT. Protein concentration was measured with a NanoDrop spectrophotometer at an absorbance of 280 nm. The following FASP protocol was carried out at RT and all centrifugation steps were done at 14'000 g [43]: In order to disrupt SDS micelles, 200 µl of UA were added to 20 µg of extracted protein and the samples were loaded onto Microcon-30 filters (Merck Millipore) and centrifuged for 20 min. Free cysteines were alkylated by the addition of 100 µl of 50 mM IAA and the samples were incubated at 600 rpm for 1 min. Samples were incubated for another 5 min on the bench and then centrifuged for 20 min. In order to wash the samples and remove SDS, 100 µl UA were added 3 times and centrifuged each time for 15 min. Then, two washes of 100 µl 0.5 M NaCl were added and the sample was centrifuged for 20 min twice. The filter units were transferred into new collection tubes and 120 µl of triethylammonium bicarbonate (TEAB) containing sequencing grade trypsin (Promega) in a 1:50 ratio of trypsin to protein (w/w) were added to the filter. Samples were mixed 1 min at 600 rpm and incubated overnight in a wet chamber. Peptides were recovered by centrifugation and the flow-through was adjusted to a final concentration of 0.5% trifluoroacetic acid (TFA). For the fractiona-

tion experiment, the same FASP protocol was followed with 300 μg protein as starting material.

StageTip clean-up. Peptides were then cleaned in self-packed C18 StageTips prior to LC-MS/MS analysis [44]. StageTips were wetted with 100% methanol (MeOH) and cleaned with 150 μl 60% acetonitrile (ACN), 0.1% TFA. They were then equilibrated with 150 μl 3% ACN, 0.1% TFA prior to sample loading. Sample volume was raised to 150 μl 3% ACN, 0.1% TFA and peptides were loaded and washed twice with 150 μl 3% ACN, 0.1% TFA before elution with 150 μl 60% ACN, 0.1% TFA in a new vial. Samples were dried to completeness by vacuum centrifugation. For the fractionation experiment, peptide cleanup was done following the same protocol on C18 SPE cartridges (Waters) with 800 μl reagent volumes.

LC-MS/MS

Method comparison. Dried peptides were resuspended in 20 μl MS sample buffer (3% ACN, 0.1% formic acid (FA) in water) and sonicated for 5 min to enhance peptide solubilization. For retention time normalization and quality control, iRT peptides (Biognosys) were added to all samples. For method optimization experiments, 1 μl of peptide solution was analyzed on a nanoAcquity UPLC (Waters) coupled to a Q Exactive mass spectrometer (Thermo Fisher Scientific). Peptides were separated by low pH reversed-phase chromatography applying a forward trap elute configuration (Acquity UPLC M-Class Symmetry C18 Trap Column, 100 Å, 5 μm, 180 μm × 20 mm, Waters, 186007496). The peptides were separated with a mixture of solvent A (0.1% FA in water) and solvent B (0.1% FA in ACN) over a 5–32% B linear gradient for 90 min at a flow rate of 300 nl/min (HSS T3 Column, 100 Å, 1.8 μm, 75 μm × 250 mm, Waters, 186008818) and with a column temperature of 50 °C. Columns were cleaned with 95% B for 5 min prior to re-equilibration for 10 min to reach initial conditions. All samples were injected in a randomized fashion and standard samples were injected every 4 samples.

Full scan MS spectra were acquired from 200 to 2000 *m/z* with an automatic gain control (AGC) target of 3e6, an Orbitrap resolving power of 70′000 and a maximum injection time of 100 ms. Internal mass calibration was performed using the lock masses 371.101 *m/z* and 445.120 *m/z*. For MS2 scans, the top 12 most abundant ions were selected for higher-energy collisional dissociation (HCD) with a normalized collision energy of 30, a quadrupole isolation window of 1.4 *m/z* and a maximum injection time of 50 ms. MS2 spectra were recorded from 200 to 2000 *m/z* at a resolving power of 17′500 with an AGC target of 1e5 and a maximum injection time of 50 ms.

Precursor ions below the intensity threshold 16′000 and ions with unassigned charge states or charges of +1 or > +8 were excluded. Dynamic exclusion was set to 10 s.

Offline high pH reversed-phase chromatography peptide fractionation. Dried peptides (100 μg) were dissolved in buffer A (4.5 mM ammonium formate, pH 10, in 2% ACN) and separated using a C18 column (XBridge Peptide BEH C18 column, 130 Å, 3.5 μm, 1 mm × 100 mm, Waters, 186003561) on an Agilent 1100 Series Capillary LC System. Buffer B was 4.5 mM ammonium formate, pH 10, in 90% ACN. The 90-minute gradient used was as follows: 0% B for 10 min, 0–40% B in 60 min, 40–100% B in 2 min, 100% B for 8 min, 100–0% B in 2 min, and 0% B for 8 min, with a flow rate of 0.1 ml/min. Fractions were collected every 3.33 min since the beginning of the gradient and the 27 fractions were pooled into 9 non-contiguous fractions (F1 + F10 + F19, F2 + F11 + F20, etc.). The fractions were dried to completeness by vacuum centrifugation and re-dissolved in 20 μl MS buffer. iRT peptides (Biognosys) were added to all pooled fractions.

In-depth proteome profiling. Peptide fractions (2 μl) were injected on a nanoAcquity UPLC M-Class System (Waters) coupled to a Q Exactive HF instrument and separated with the following gradient: 5–40% B in 90 min, 95% B for 5 min, 5% B for 10 min by low pH reversed-phase chromatography on a C18 column (Acquity UPLC M-Class HSS T3 C18 column, 1.8 μm, 75 μm × 250 mm, Waters, 186007474) at 50 °C. Samples were injected in a randomized order and a standard sample was injected every 4 samples for quality control. Full scan MS spectra were acquired from 350 to 1500 *m/z* with an AGC target of 3e6, an Orbitrap resolving power of 120′000 and a maximum injection time of 50 ms. Internal mass calibration was performed using the lock masses 371.101 *m/z* and 445.120 *m/z*. For MS2 scans, the top 24 most abundant ions were selected for higher-energy collisional dissociation (HCD) with a normalized collision energy of 28, a quadrupole isolation window of 1.2 *m/z* and a maximum injection time of 50 ms. MS2 spectra were recorded from 200 to 2000 *m/z* at a resolving power of 30′000 with an AGC target of 1e5 and a maximum injection time of 50 ms. Precursors below the intensity threshold of 16′000 and ions with unassigned charge states or charges of +1 or above +5 were excluded. Dynamic exclusion was set to 15 s.

Bioinformatics analysis

Database searches and statistical filtering. For the protocol comparison, the raw files of the 6 samples were loaded in MaxQuant (v1.6.2.3) and

a label-free quantification using intensity-based absolute quantification (iBAQ) [45] was selected. Trypsin/P was selected as enzyme and carbamidomethylation of cysteine was selected as fixed modification and oxidation of methionine and deamidation of asparagine and glutamine as variable modifications. A protein False Discovery Rate (FDR) of 0.05 and match between runs were selected as parameters for the analysis. The output MaxQuant file was restricted to a minimum of 2 unique peptides. For the identification of quantitative data from the fractionated and non-fractionated samples, the raw files of the 9 fractions were loaded in MaxQuant (v1.6.2.3) and label-free quantification using iBAQ [45] was selected. Trypsin/P was selected as enzyme, carbamidomethylation of cysteine was selected as fixed modification and oxidation of methionine and deamidation of asparagine and glutamine as variable modifications. A protein FDR of 0.05 and match between runs were selected as parameters for the analysis. The same parameters were used for the analysis of the individual single shot run. The list of proteins identified in the MaxQuant output file was restricted to a minimum of 2 unique peptides.

Gene-set enrichment analysis (GSEA) and over-representation analysis (ORA). For the fractionation experiment, a GSEA was performed ranking the identified proteins by the logarithmic transformation (base 2) of the iBAQ value and an ORA was done to compare the proteins identified by fractionated vs non-fractionated. Both analyses were done in the WEB-based GEne SeT AnaLysis Toolkit platform (WebGestalt; www.webgestalt.org) [46]. For identification of ECM proteins, the Human Matrisome Project [47,48] was searched. Venn Diagrams were generated with Biovenn [49].

Comparison with previously reported RNA sequencing data. To evaluate the depth of our proteomics experiment we compared our data to previously published RNA sequencing data (RNA-seq). For this, the data from https://www.ebi.ac.uk/ena/data/view/PRJNA316992 were downloaded and reanalyzed. The RNA-seq reads were aligned with the STAR-aligner. As reference, we used the Ensembl human genome build GRCh38.p13 using the gene annotation as provided by GENCODE 32 release. Gene expression values were computed with the function featureCounts from the R package Rsubread [50]. Only the control samples were used for the comparison to the proteomics data. To achieve a good mapping from Ensembl Gene Identifier (ENSG) to Ensembl Protein Identifier (ENSP) we used the human Ensembl AA-FASTA where ENSP are all listed with the respective ENSG number. To identify what transcripts were identified in our mass spectrometry analysis as proteins, the two datasets were merged using the ENSG number. The average transcripts per million (TPM) were averaged for all control samples of the respective study, and values of zero were omitted.

Statistical analysis

The fold changes and p-values were calculated using the protein groups output file from MaxQuant. A set of functions implemented in the R package SRMService [51] was used to perform moderated t-tests [52] for all proteins quantified with at least 2 peptides, employing the R package limma [53]. Volcano plots and heatmaps were created with R (v.3.6.1) and RStudio (v.1.2.1578) using the gplots library [54].

Immunohistochemical analysis (IHC)

For IHC, FMs were sandwiched in IHC cassettes, fixed in 4% formalin, embedded in paraffin and consecutive sections of 4 μm were prepared. Slides were then deparaffinized and rehydrated, and different heat-mediated antigen retrieval methods were performed according to the manufacturer's guidelines (Table S6). Sections were then blocked for 1 h at RT in 1.5% bovine serum albumin (BSA)/PBS containing 0.5% Tween-20, and the primary antibody was incubated overnight at 4 °C in blocking solution in a humidified chamber. The next day, sections were rinsed three times with 0.1% Tween-20/PBS and were incubated the corresponding secondary antibody in blocking solution for 5 h at RT. Then, the peroxidase substrate ImmPACT© AMEC Red (Vector Laboratories) was applied to the slides for the suitable time, and the sections were counterstained with hematoxylin (Vector Laboratories) and mounted in glass slides in mounting medium (Abcam). A coverslip was added on top and slides were imaged on an inverted Zeiss microscope. Images were processed with Fiji from ImageJ [55,56].

Results and discussion

Quantification of filter-aided sample preparation (FASP) and urea-based sample preparation reveals preparation-dependent patterns

ECM proteins are hard to solubilize and, for this reason, an adequate sample preparation strategy must be chosen in order to obtain a comprehensive characterization of the ECM of a tissue. Consequently, we first compared two methods known to be suitable for the preparation of samples with insoluble proteins for LC-MS/MS. One method is a traditional urea-based protein extraction and in-solution protein digestion (in the following referred to as 'urea-based sample preparation') [57], while the other method is based on the extraction of proteins by the detergent

sodium dodecyl sulfate (SDS) followed by a proteolytic digestion on a filter (filter-aided sample preparation; FASP) [43] (Fig. 2). For this, ground amnion tissue was divided into three batches and peptide preparation and LC-MS/MS analysis were performed for both methods in triplicates.

After sample preparation and LC-MS/MS analysis, data was analyzed in MaxQuant [58] by label-free and intensity-based absolute quantification (iBAQ) [45]. In total, 1286 proteins were identified with an estimated false discovery rate (protein FDR) of 0.85%. In order to decipher extraction patterns between the two sample preparation methods, we determined the relative abundance of the identified proteins and depicted the transformed intensities in a heatmap (Fig. S1A). An analysis of the proteins identified by each extraction revealed a high reproducibility of both methods (Fig. S1B).

To characterize the differences in protein extraction by the two methods, we generated a volcano plot (Fig. 3A). To assert that a protein was more efficiently solubilized with one of the two methods, we defined a threshold of fold change of 2 in protein abundance (calculated by the normalized transformed intensities), and a minimum adjusted p-value of 0.05. Following these criteria, 155 proteins (12%) were more abundant in the FASP samples, while 96 proteins (6%) were significantly better prepared using the urea-based method (Fig. 3A). Given the

importance of preserving the ECM integrity throughout pregnancy and the variety of cell functions that the ECM controls [59], we specifically investigated the influence of the protein preparation method in the extraction of ECM proteins. To do so, we cross-referenced our identified proteins with the Human Matrisome Project [48] and identified 133 ECM proteins [60]. Of these, 69 proteins were better prepared by FASP, and 64 were better prepared by urea, as visualized by a heatmap of the intensities (Fig. 3B). In particular, 15 ECM proteins (11% of the total identified ECM proteins) were significantly more abundant in the samples prepared by the FASP method and 9 (7%) were more significantly more abundant in the urea-based prepared samples (Fig. 3A and Tables S1 and S2). The superior solubilization of proteins by FASP led us to select it as the method of choice for investigating the amnion proteome in depth.

Increasing the human amnion proteome coverage by the use of a multidimensional proteomic strategy

Due to the intrinsic complexity of the human proteome and the limitations of unidimensional shotgun proteomics, orthogonal peptide separation has been included in proteomic pipelines to increase proteome coverage [61]. Therefore, to gain a deeper understanding of the
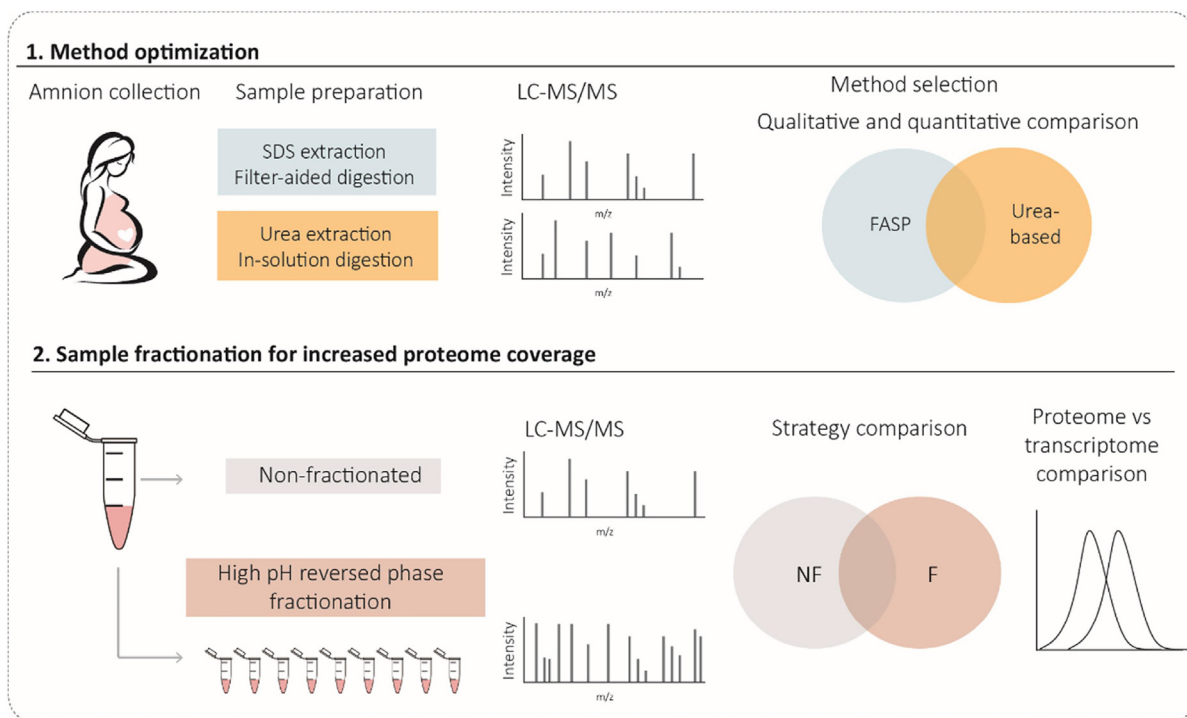

Fig. 2. Workflow of the project. 1) Method optimization was done by comparing filter-aided sample preparation (FASP) and urea-based sample preparation. 2) Further sample fractionation prior to LC-MS/MS enabled deep profiling of the amnion proteome. The proteome data was compared to transcriptomic data of the amniotic membrane.
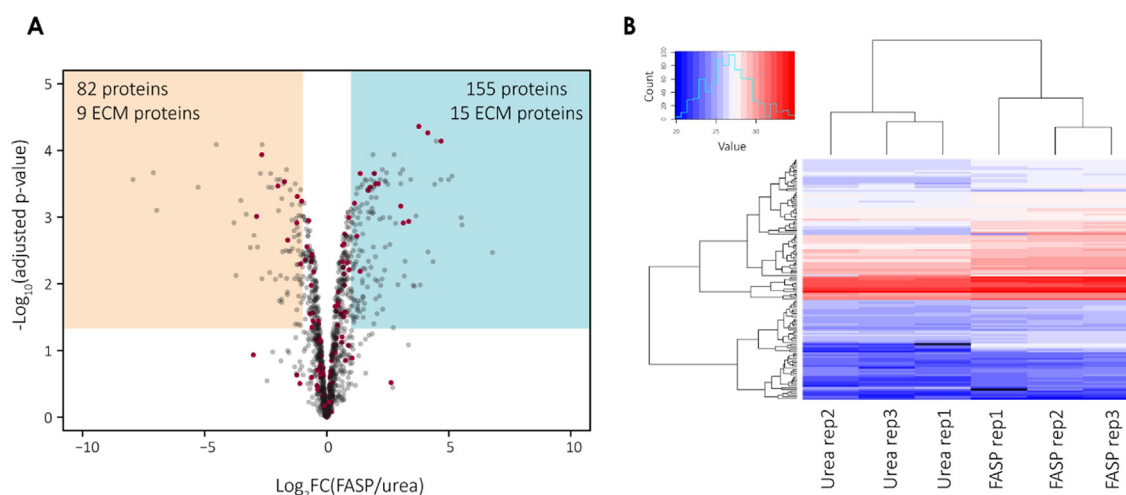
Fig. 3. Comparison of FASP and urea-based sample preparation methods. A) Volcano plot showing the significance of protein identifications versus the mean fold change of FASP/urea-based. Blue and orange areas indicate where the thresholds are met (fold change ≥ 2 with an adjusted p-value ≤ 0.05) for FASP (blue) and urea (orange), respectively. Proteins assigned to the ECM are depicted by red dots, those not associated to the ECM are shown in grey dots. B) Heatmap depicting ECM protein intensities as Log_2 (raw intensity value). (For interpretation of the references to color in this figure legend, the reader is referred to the web version of this article.)

human amnion proteome, we introduced a high pH reversed-phase liquid chromatography (RP-HPLC) fractionation step prior to LC-MS/MS, from which 27 fractions were non-contiguously pooled in groups of 3. The resulting 9 fractions were separated over the same gradient as the single-shot sample. Interestingly, the number of proteins identified with more than 2 unique peptides in the fractionated sample was 2.7-fold higher than the number of proteins identified in the single-shot injected sample, with 5528 and 2066, respectively (Tables S3 and S4). A comparison of the two lists revealed 1986 shared proteins, 77 proteins solely identified with the single-shot strategy, and 3542 exclusives in fractionated sample (Fig. S2A). The substantial increase in protein identifications by the concatenation of high and low pH chromatography steps prior to MS/MS analysis is in line with the earlier published MCF10A human breast epithelial cell line proteome, where identifications on a peptide and protein level increased by 1.8- and 1.6-fold, respectively [62]. Next, to understand if sample fractionation leads to the more efficient identification of specific types of proteins, we categorized them by the different 'Cellular Component' GO categories. We observed that sample fractionation resulted in a global and unbiased increase in protein identifications for all categories (Fig. S2B).

Overall, the number of protein identifications in our study is far superior to previously reported research of the human amnion. An earlier proteomic study on the FMs identified 92 soluble proteins and 19 membrane proteins by using 2-dimensional gel electrophoresis followed by MALDI-TOF [38]. Other studies have evaluated the effect of cryopreservation in the transplant-ready amniotic membrane (TRAM) [39] and reported 70 proteins to be affected by handling. A study focusing on epithelium-denuded amniotic membrane [40] identified 43 highly abundant proteins by Matrix Assisted Laser Desorption/Ionization (MALDI-TOF). More recent work [36] compared the soluble proteins of fresh and cryopreserved human amniotic membranes by isobaric tagging for relative quantification (iTRAQ) and identified 1949 soluble proteins that were unaltered by cryopreservation.

After characterizing and quantifying the amnion proteome, we sought to determine the similarity of our data with previously reported transcriptional profiling data. For this, we compared our proteomics data with data from 12 control donors from a previous publication [63] that is available in the European Nucleotide Archive (ENA database) (Fig. 4A). Based on the more sensitive RNA sequencing (RNA-seq) technique where transcripts can get amplified and it is assumed that with this technique no transcripts are missed, we can assume that our proteomics dataset covers more than 40% of all the expressed transcripts for this tissue. When we distributed the identified proteins (depicted in blue) and missed transcripts (depicted in pink) across the mean expression of the identified transcripts (Fig. 4A, top panel) we observed that proteins were better identified in the higher expressed ranges. This is underlined by looking at the fraction of identified proteins per bin (Fig. 4A, middle panel) where around 70–75% of all the transcripts were identified in these bins, while for lower expressed transcripts gradually less proteins
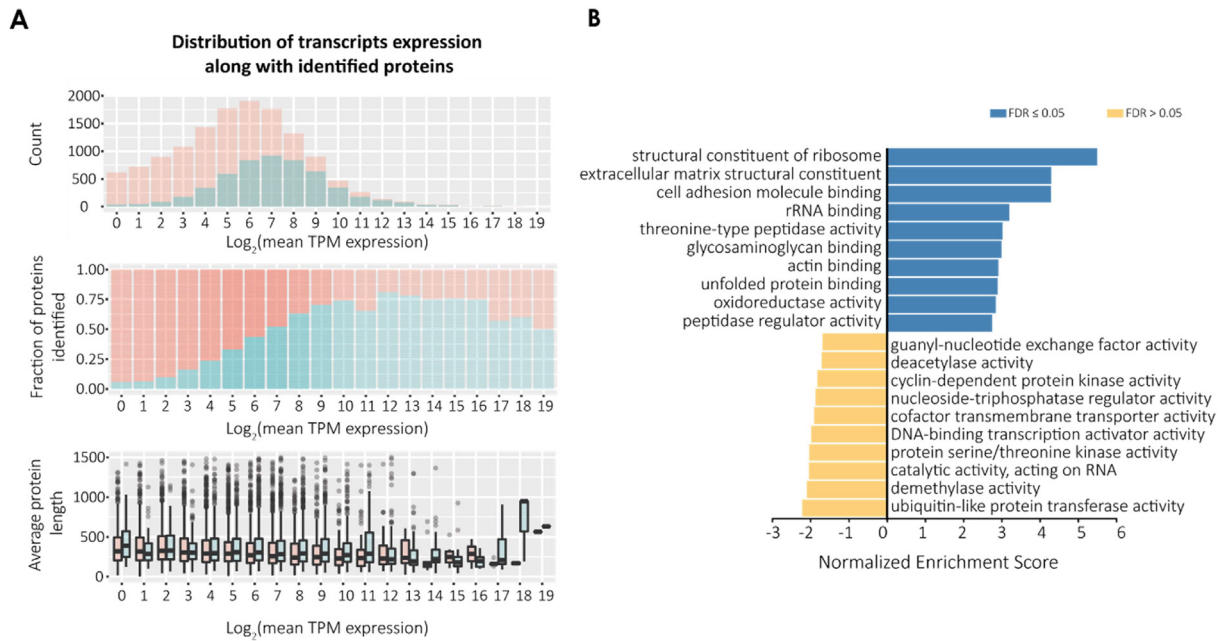
Fig. 4. In-depth proteomic characterization of the amniotic membrane. A) Comparison of our proteomics dataset with previously reported RNA sequencing data of the human amnion. Top panel: Histograms showing the distribution of the identified proteins (depicted in blue) and missed transcripts (depicted in pink) across the mean expression of the identified transcripts. Middle panel: Fraction of identified proteins per bin, according to the mean TPM expression. Lower panel: Average protein length versus the mean transcripts per million (TPM) expression. B) A Gene-Set Enrichment Analysis (GSEA) showing the enriched categories in the amnion proteome by the 'Molecular Function' category. (For interpretation of the references to color in this figure legend, the reader is referred to the web version of this article.)

were identified. Splitting the transcripts in each bin into "identified as proteins" or "not identified as proteins" (Fig. 4A, bottom panel) and showing the length distribution, we observed that, in general, the identified proteins were often a bit longer than the proteins that were missed (however, not significantly). This indicates that there is no particular length bias in the identifications, also not for genes where the transcript is only weakly expressed.

To decipher the most abundant protein categories in the amnion we undertook a gene-set enrichment analysis (GSEA) with ranked $\log_2$(iBAQ values) by the Gene Ontology (GO) 'Biological Process', 'Molecular Function' and 'Cellular Component' (Fig. 4B and Fig. S3). The GSEA by the 'Molecular Function' GO revealed 'structural constituent of ribosome' as the most enriched category. Interestingly, 'extracellular matrix structural component' and 'cell adhesion molecule binding were the 2nd and 3rd most enriched categories, with a size of 87 and 326 proteins and a 4.296 and 4.285 normalized enrichment score (NES), respectively ($p < 0.00010$, FDR < 0.00010; see 'statistical analysis' section for details) (Fig. 4B and Fig. S3).

Characterization and relative quantification of the term amnion matrisome

Next, we cross-referenced the proteins identified in the human amnion with the Human Matrisome Project [60]. This classification of the ECM proteins includes the identification of core matrisome and matrisome-associated proteins. Core matrisome proteins are the building blocks of the ECM and consist of collagens, proteoglycans and glycoproteins. On the other hand, matrisome-associated proteins comprise ECM-affiliated proteins, regulators and secreted factors that work in close contact with ECM core proteins and participate in the maintenance and remodeling of the ECM. With our approach, we identified 117 core ECM proteins and 168 matrisome-associated proteins (Table S5). This is a significantly higher number than previous similar reports in which 47 core ECM proteins and 63 matrisome-associated proteins were identified [36]. We hypothesize that the higher number of ECM proteins can likely be attributed to the applied extraction method, that is not only extracting soluble proteins, and to the used instrument.

Next, we quantified the ECM signal volumes relative to the total signal volume. This

quantification of all signal volumes revealed that the ECM protein abundance was approximately 20% of the total protein abundance (Table 1). Furthermore, a ranking of the identified proteins by iBAQ protein abundance revealed an even distribution of ECM protein identifications throughout the dataset (Fig. 5A).

We then further deciphered the distribution of proteins in the different ECM categories according to their abundance. When ranking the ECM categories by summed abundance relative to the total ECM protein abundance, the most abundant ECM proteins were ECM-affiliated proteins (26.88%), closely followed by secreted factors (26.39%). ECM glycoproteins (18.50%) and proteoglycans (11.65%) were intermediate in abundance, and ECM regulators represented a 9.45% of the total signal volume. Surprisingly, collagens (7.13%) were the least abundant category of ECM proteins (Fig. 5B). Our study indicates that the FMs, additionally to being a collagen-rich tissue as previously reported [1], contain a broad spectrum of other ECM components. We hypothesize that the difficulty of extracting and digesting collagens and the high number of cellular identifications should not be excluded as potential causes of mismatch with previously published reports. Nonetheless, our detailed characterization of the amnion ECM composition and relative abundance is an important step towards the understanding of the FM composition.

Among the top 10 iBAQ-ranked core matrisome proteins, transforming growth factor-beta-induced protein ig-h3 (TGFβI), dermopontin (DPT), microfibril associated protein 2 (MFAP2), and fibrillin-1 (FBN1) were the most abundant ECM glycoproteins identified (Table 2). TGFβI has previously been reported as one of the most abundant proteins in the amniotic membrane [39]. It is an ECM adhesive molecule that acts as a membrane-associated growth factor in processes like cell growth, differentiation and wound healing [39]. An immunohistochemical analysis revealed the ubiquitous distribution of TGFβI in the mesenchyme of the amniotic membrane, underlying the epithelial basement membrane (Fig. 5C).

Table 1 Quantification of ECM protein abundance.

Category	iBAQ sum	% of total signal
Core matrisome	**6.98E+09**	**7.45%**
Collagens	1.33E+09	1.42%
Proteoglycans	2.18E+09	2.33%
ECM Glycoproteins	3.46E+09	3.70%
Matrisome-associated	**1.17E+10**	**12.53%**
ECM-affiliated Proteins	5.03E+09	5.37%
ECM Regulators	1.77E+09	1.89%
Secreted Factors	4.94E+09	5.27%
ECM proteins	**1.87E+10**	**19.98%**
No assigned category	7.50E+10	80.02%
Total abundance	9.37E+10	

The proteoglycans decorin (DCN), lumican (LUM), mimecan (OGN), prolargin (PRELP), biglycan (BGN) and proteoglycan 2 (PRG2) were identified as highly abundant FM components. Decorin has been previously described in the human amnion [72] and has been the focus of studies related to PPROM, as it has been shown that decorin-defficient mice deliver their pups prematurely [73]. Furthermore, decorin has been reported to be involved in pathways related to the maintenance of FM integrity [74], as it is involved in collagen fibrilogenesis [75]. Despite its known presence in the FMs, its abundance in the amnion was never described before. Lumican is a small leucine-rich proteoglycan (SLRP) that has been previously reported to be present in the compact layer of the amnion [76] and to play a role in epithelial cell migration and tissue repair. Indeed, a confirmation of these identifications by IHC revealed decorin in the epithelial cell junctions, and lumican mostly expressed in the vicinity of the amnion stromal cells (Fig. 5C). Additionally, we identified several matrisome-associated proteins, classified into ECM-affiliated proteins, ECM regulators and secreted factors (Table 3). Among the top 10 ECM-affiliated proteins several annexins (ANXA1, ANXA2, ANXA3 and ANXA4) were identified, as well as galectin-3. Annexins I and II have been previously reported to be present in the fetal membranes, specifically in the amnion epithelial cells and in the fibroblasts of the fibroblast layer. They are known to be involved in the regulation of several cellular functions, including secretory processes and anti-inflammatory responses [39,77]. Furthermore, annexin A1 has been reported to promote resolution of inflammation and wound healing, and to interact with S100-A11. Indeed, IHC revealed a co-localization of the proteins in the cytoplasm and the surroundings of both amniotic stromal and epithelial cells (Fig. 5C). Among other secreted factors, we identified S100-A4, which has been reported to be involved in wound healing. Strikingly, protein S100-A4 was the 2nd most abundant matrisome-associated protein and the 5th most abundant protein identified in the full dataset (based on iBAQ protein abundance ranking). The IHC analysis showed that it was highly expressed both in the epithelial layer and the stroma of the amniotic membrane (Fig. 5C).

Confirmation of tissue-remodeling proteins by IHC

We next undertook a careful and detailed analysis of our dataset in order to find other players known to be involved in wound healing and tissue remodeling. This approach revealed the identification of several MMPs and TIMPs in the human amnion. It has been previously reported that, during the course of pregnancy, the FMs maintain their integrity through a homeostatic balance between matrix metalloproteinases
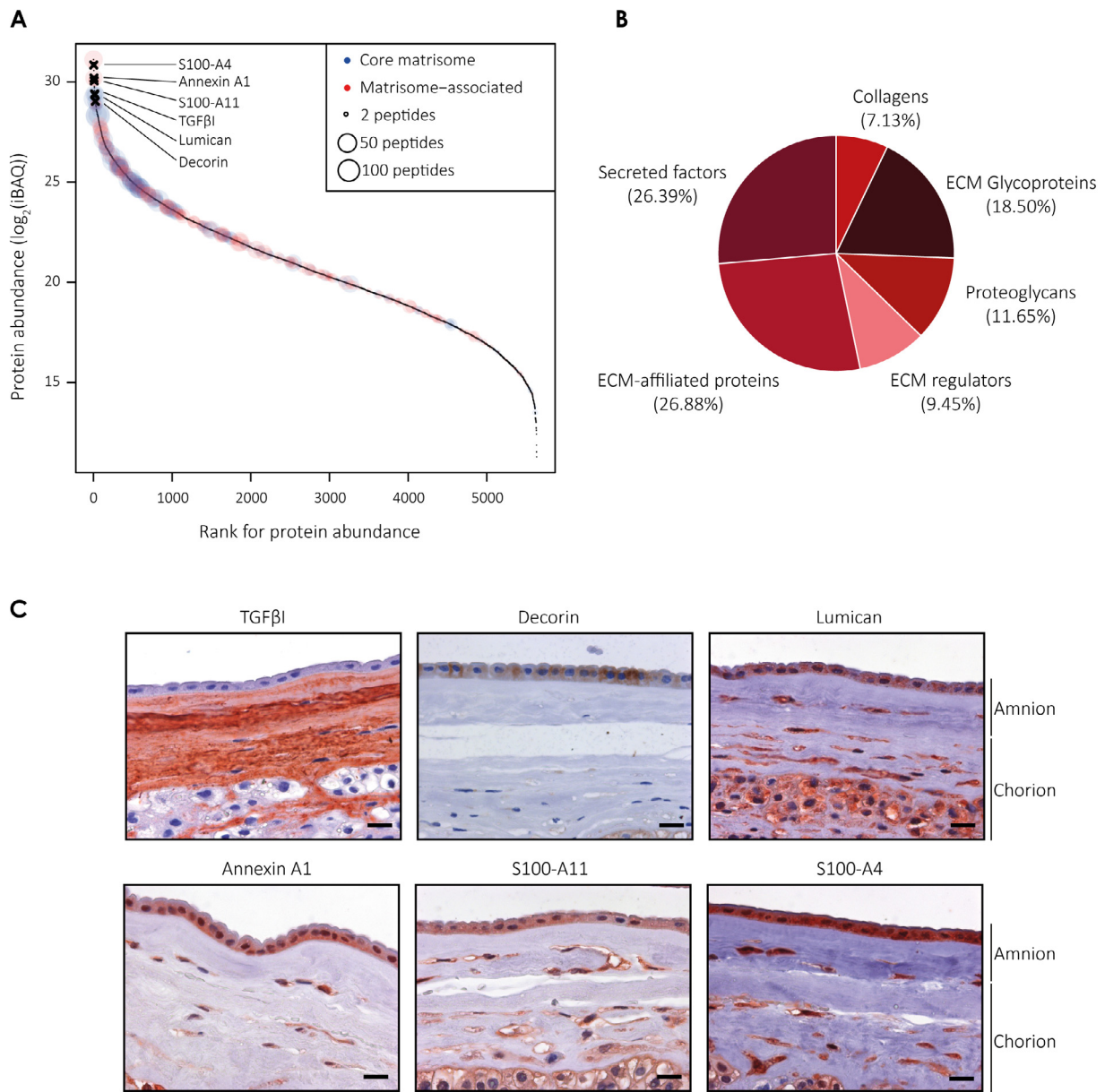
A

B

C

Fig. 5. Characterization of the human amnion ECM. A) Quantification of the iBAQ abundance of the ECM proteins through the rank of identified proteins. B) Abundance of the identified ECM proteins, over the total signal corresponding to ECM proteins. C) Core matrisome and matrisome-associated proteins identified by proteomics were confirmed by IHC. Nuclei were counterstained with hematoxylin. Scale bars are 20 μm.

(MMPs) and the tissue inhibitors of MMPs (TIMPs) [5]. Several MMPs were identified (MMP2, MMP10, MMP14, MP19 and MMP23b) which had, except MMP2 and MMP10 [27], to our knowledge never been reported before (Table 4). MMP2 and MMP9 have been previously reported to be regionally present both in the amnion and the chorion [26]. MMP10, on the opposite, has been reported to be present in the amnion and the chorion by in-situ hybridization [27], but its localization in the FMs has, to our knowledge, never been shown before. By IHC, we assessed the localization of MMP10, which was shown to be expressed both by epithelial and mesenchymal amniotic cells. MMP10, also called stromelysin-2, is an MMP that is known to degrade fibronectin, denatured collagen types I, III, IV, and V and native collagen types III, IV, and V [81]. We newly identified MMP14, a membrane-bound endopeptidase that is known to degrade a variety of ECM components, such as collagen. Most importantly, its essential role in the development of skeletal and extraskeletal connective tissues during development and in pericellular collagenolysis has been reported [81]. By IHC, we observed that MMP14 was specifically localizing in the basement membrane of the epithelial cells and in the

Table 2 Top 10 core matrisome proteins identified in the human amniotic membrane, their abundance and their functions as reported in the String DB [71], unless otherwise noted. Color coding on the left: ECM glycoproteins (green), proteoglycans (red) and collagens (orange).

	Protein	Gene	iBAQ	Rank	Function
🟩	Transforming growth factor-beta-induced protein ig-h3	TGFβI	7.08E+08	21	Has been described to participate in several physiological processes such as morphogenesis, cell migration, angiogenesis and inflammation [64]
🟥	Lumican	LUM	6.87E+08	22	Plays a role in epithelial cell migration and tissue repair and in collagen fibrillogenesis and maturation [65]
🟥	Decorin	DCN	5.48E+08	30	May affect the rate of collagen fibril formation. Plays a role in tissue development and assembly [66]
🟩	Dermatopontin	DPT	5.30E+08	32	Seems to mediate adhesion by cell surface integrin binding. Enhances TGFβI activity and interacts with decorin. Inhibits cell proliferation and accelerates collagen fibril formation [67]
🟥	Mimecan	OGN	4.87E+08	34	Plays a pivotal role in collagen fibrillogenesis in the skin
🟩	Microfibril associated protein 2	MFAP2	3.80E+08	51	Plays a role in microfibril assembly, elastinogenesis and tissue homeostasis [68]
🟧	Collagen VI α1	COL6A1	3.44E+08	60	Acts as a cell-binding protein and as an anchor of the basement membrane to the surrounding ECM. Plays a major role in skeletal muscle and regulates autophagy [69]
🟩	Fibrillin-1	FBN1	3.37E+08	62	Structural component of the 10–12 nm diameter microfibrils of the ECM, which conveys both structural and regulatory properties to load-bearing connective tissues. It is known to act as a template for elastin deposition [70]
🟧	Collagen VI α3	COL6A3	3.29E+08	64	Acts as a cell-binding protein and as an anchor of the basement membrane to the surrounding ECM. Plays a major role in skeletal muscle and regulates autophagy [69]
🟧	Collagen VI α2	COL6A2	1.94E+08	105	Acts as a cell-binding protein and as an anchor of the basement membrane to the surrounding ECM. Plays a major role in skeletal muscle and regulates autophagy [69]

Table 3 Top 10 matrisome-associated proteins identified in the human amniotic membrane, ranked by their abundance and their functions as reported in the String DB [71], unless otherwise noted. Color coding on the left refers to: ECM-affiliated proteins (yellow), secreted factors (blue) and ECM regulators (grey).

	Protein	Gene	iBAQ	Rank	Function
🟨	Annexin A2	ANXA2	2.32E+09	3	Facilitates ECM degradation through its ability to simultaneously interact with the cytoskeletal, membrane and ECM components [78]
🟦	Protein S100-A4	S100-A4	1.92E+09	5	May play a role in corneal wound healing [79]
🟨	Annexin A1	ANXA1	1.22E+09	9	Promotes resolution of inflammation and wound healing [80]
🟦	Protein S100-A6	S100-A6	1.15E+09	12	May function by interacting with other proteins and indirectly play a role in many physiological processes such as the reorganization of the actin cytoskeleton and in cell motility
🟦	Protein S100-A11	S100-A11	1.11E+09	13	Is known to interact with annexin 1 and to play a role in a variety of cellular events including differentiation, signaling and migration
🟦	Protein S100-A10	S100-A10	5.09E+08	33	Is known to interact with annexin 2 and to play a role in a variety of cellular events including differentiation, signaling and migration
🟨	Galectin-3	LGALS3	4.76E+08	36	Involved in acute inflammatory responses including neutrophil activation and adhesion
⬜	Alpha-1-antitrypsin	SERPINA1	2.47E+08	82	Inhibitor of serine proteases. Its primary target is elastase, but it also has a moderate affinity for plasmin and thrombin. Irreversibly inhibits trypsin, chymotrypsin and plasminogen activator
🟨	Annexin A4	ANXA4	2.18E+08	97	Calcium/phospholipid-binding protein which promotes membrane fusion and is involved in exocytosis
🟨	Annexin A3	ANXA3	2.12E+08	99	Inhibitor of phospholipase A2, also possesses anti-coagulant properties. Also cleaves the cyclic bond of inositol 1,2-cyclic phosphate to form inositol 1-phosphate

Table 4 MMPs and TIMPs identified in the amnion proteome analysis. Proteins marked with an asterisk (*) sign are novel identifications.

Protein	Gene	iBAQ	Rank
Metalloproteinase inhibitor 3	TIMP3	2.72E+07	567
Metalloproteinase inhibitor 1	TIMP1	2.45E+07	614
Matrix metallopeptidase 19*	MMP19	7.22E+06	1361
Matrix metallopeptidase 2	MMP2	2.04E+06	2482
Matrix metallopeptidase 10	MMP10	1.41E+06	2817
Metalloproteinase inhibitor 2	TIMP2	1.01E+06	3164
Matrix metallopeptidase 14*	MMP14	6.80E+05	3560

surrounding of mesenchymal stromal cells (Fig. 6A). Last, we identified MMP19, an endopeptidase known to be able to degrade a variety of components on the ECM [81] specifically localizing in the epithelial layer and in the stromal cells, with a weaker expression (Fig. 6A and Fig. S4).

TIMPS are specific inhibitors of MMPs that play an important role in wound healing and the regulation of cell migration. TIMP1, TIMP2 and TIMP3, which have as well been reported to control ECM remodeling [28], were identified with our proteomic approach. TIMPs 1–4 have been previously reported to be found in the human amnion, and their localization has been shown by IHC [82].

The ECM proteins are known to bind growth factors, which are critical for tissue repair and are capable of eliciting cellular responses and guiding cellular behavior [24]. During the wound healing response, growth factors which regulate a cascade of events are produced. The identification of 32 growth factors and receptors is reported, many of which had never been reported before (Table 5).

From our list of new identifications, we selected heparin binding growth factor (HDGF), latent transforming growth factor beta binding protein 1 (LTβP1) and platelet-derived growth factor D (PDGFD) and confirmed their presence by IHC (Fig. 6B and Fig. S4). HDGF has been shown to have mitogenic activity for fibroblasts [71] and was more strongly expressed by amnion mesenchymal stromal cells than by epithelial cells. Given the high levels of expression of TGFβI in the amnion, we were interested in deciphering the localization of LTβP1, which is a key regulator of proteins of the transforming growth factor beta family (TGFβ1, TGFβ2 and TGFβ3). By controlling their activation by maintaining them in a latent state during storage in extracellular space, LTβP1 is thought to be involved in the assembly, secretion and targeting of TGFβ1 [81]. LTβP1 was ubiquitously expressed both by the epithelial and mesenchymal cells of the amnion. LTβP1 and LTβP2 have as well been reported to be involved in elastic fiber assembly, together with MFAP2 and FBN1, two very abundant glycoproteins, and several lysyl oxidase (LOXL) proteins (Table S5), which are the enzymes responsible for the initiation of collagen and elastin cross-links [83]. However, despite it has been previously
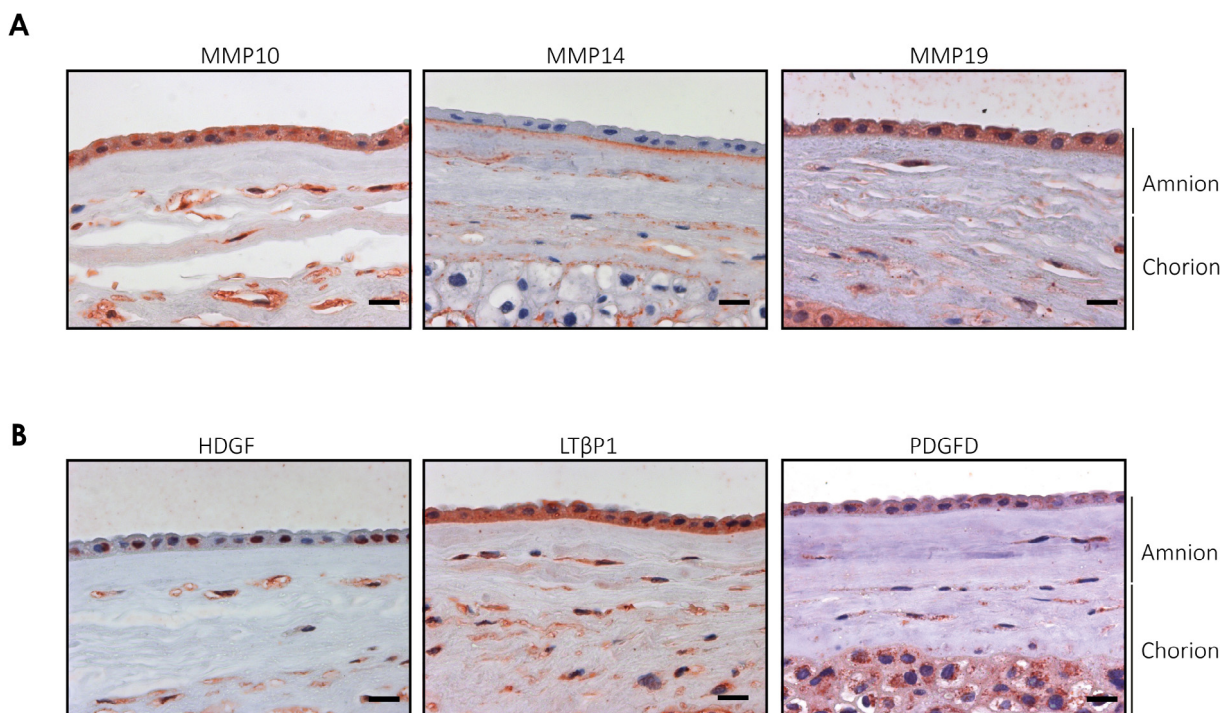

Fig. 6. Identification and localization of novel proteins in the human amnion. A) The localization of MMP10 and of the newly-identified MMP14 was reported by IHC. B) The identification and localization of novel proteins in the amnion was confirmed by IHC. Nuclei were counterstained with hematoxylin. Scale bars are 20 μm.

Table 5 Growth factors and growth factor receptors identified in the in the amnion proteome analysis. Proteins marked with an asterisk (*) are novel identifications.

Protein	Gene	iBAQ	Rank
Heparin binding growth factor*	HDGF	5.88E+07	306
Latent transforming growth factor beta binding protein 4	LTβP4	3.23E+07	490
Myeloid derived growth factor	MYDGF	3.17E+07	500
Insulin like growth factor binding protein 1	IGFBP1	2.75E+07	562
Insulin like growth factor binding protein 3	IGFBP3	1.77E+07	794
Latent transforming growth factor beta binding protein 1	LTβP1	1.39E+07	924
Latent transforming growth factor beta binding protein 2*	LTβP2	1.29E+07	976
Hepatocyte growth factor-regulated tyrosine kinase	HGS	9.57E+06	1149
Epidermal growth factor receptor	EGFR	7.99E+06	1299
Platelet derived growth factor D*	PDGFD	6.10E+06	1504
Growth factor receptor bound protein 2	GRB2	4.46E+06	1762
Wnt family member 5A	WNT5A	3,808,900	1878
Insulin like growth factor binding protein 2*	IGFBP2	3.57E+06	1941
Insulin like growth factor 2 mRNA binding protein 3*	IGF2BP3	3.28E+06	2011
Insulin like growth factor 2 mRNA binding protein 2	IGF2BP2	3.18E+06	2056
Epidermal growth factor receptor pathway substrate 15 like 1	EPS15L1	2.62E+06	2224
Epidermal growth factor receptor pathway substrate 15	EPS15	1.44E+06	2801
Frizzled class receptor 1	FZD1	1,307,100	2883
Insulin like growth factor binding protein 7	IGFBP7	1.15E+06	3032
Insulin like growth factor binding protein acid labile protein*	IGFALS	1.07E+06	3106
Fibroblast growth factor 2	FGF2	9.64E+05	3216
Insulin like growth factor binding protein 4*	IGFBP4	9.06E+05	3286
Transforming growth factor beta-1-induced transcript 1 protein*	TGFβ1I1	8.58E+05	3337
Insulin like growth factor 2 receptor*	IGF2R	6.67E+05	3587
Growth factor, augmenter of liver regeneration*	GFER	5.97E+05	3685
Platelet derived growth factor subunit B	PDGFB	5.44E+05	3784
Insulin like growth factor 1 receptor*	IGF1R	5.14E+05	3832
Wnt family member 2	WNT2	419,870	3992
Frizzled class receptor 6	FZD6	328,230	4181
Transforming growth factor beta receptor 2	TGFβR2	3.26E+05	4204
Opioid growth factor receptor*	OGFR	2.96E+05	4291
Latent transforming growth factor beta binding protein 3*	LTβP3	2.52E+05	4433
Wnt family member 7A	WNT7A	164,840	4717
Transforming growth factor beta receptor associated protein 1*	TGFβRAP1	1.65E+05	4734
Hepatocyte growth factor	HGF	1.33E+05	4865
Insulin like growth factor 2 mRNA binding protein 1	IGF2BP1	1.32E+05	4871
Wnt family member 11	WNT11	111,470	4942
Transforming growth factor beta receptor 1*	TGFβR1	1.04E+05	4994

reported to be present in the amnion both by RT-qPCR and IHC methods [84], we did not identify elastin. The reason for this might be its high degree of crosslinking, which makes it resistive to proteolytic degradation and extremely insoluble [85,86].

PDGFD, on the other hand, is a growth factor that plays a fundamental role in the regulation of embryonic development, cell migration and proliferation, survival and chemotaxis. It has been reported to be a potent mitogen for mesenchymal cells and to preferentially signal through the PDGF receptor β [87]. PDGFD was shown to be expressed both by the epithelial cells and the mesenchymal stromal cells (Fig. 6B).

Conclusions and outlook

Here we report, for the first time, a global and robust approach to characterize and quantify the protein composition of the amniotic membrane. For this, we have developed a protocol that can also be used to characterize FM of complicated, pathological or preterm pregnancies by proteomics. By analyzing the full tissue, we precluded the expected large loss of matrisome-associated proteins, specially of secreted factors, during the decellularization process. Indeed, our analysis comprised a high number of identifications both for core matrisome components and matrisome-associated proteins (Fig. 7). The presence of earlier described high abundant proteins and newly identified proteins, which likely have regulatory functions, shows the value of proteomics in the understanding the physiology of the FMs.

Furthermore, we identified novel factors that are known to be involved in wound healing. These novel identifications, together with the identifications of novel growth factor receptors, are a promising starting point for the development of biochemically-defined materials for FM regeneration. The importance of MMPs in tissue
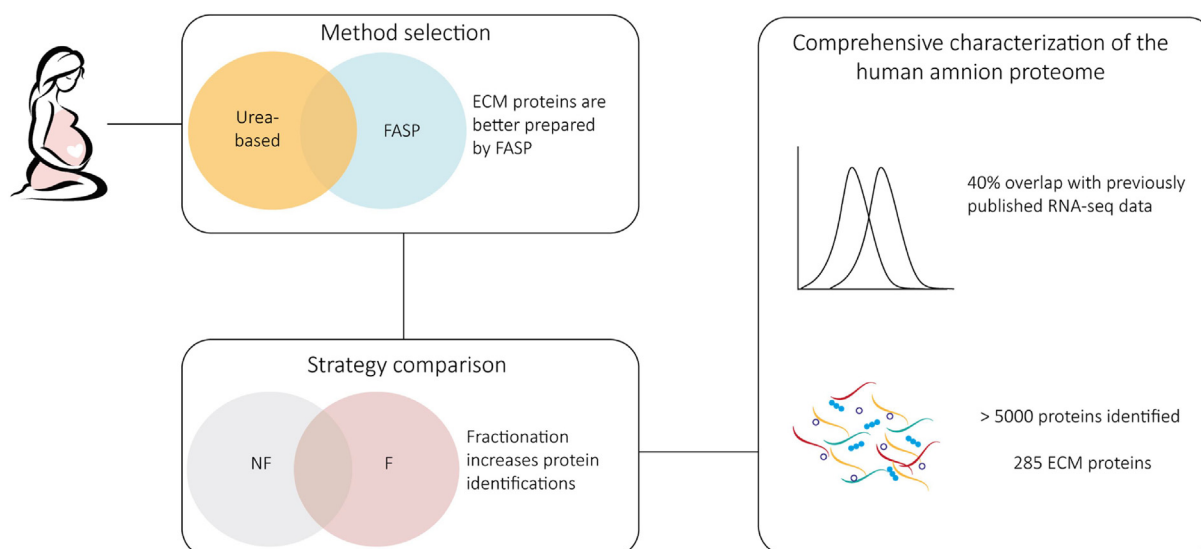
Fig. 7. Summary of the findings of the study.

remodeling is well known in the field of biomaterials, as several previously developed strategies have incorporated MMP-cleavable sites with the aim of enabling cell migration and material remodeling [88]. Furthermore, the feasibility of tuning the MMPs/TIMPs balance was demonstrated by the development of an MMP-cleavable hydrogel loaded with TIMP3, which would trigger a negative loop response in the event of hydrogel degradation [89]. Repair-promoting biomaterials have as well been engineered by combining the sequential release of MMP for wound edge softening followed by the release of the chemoattractant PDGF-AB for dense connective tissue repair [90]. Recently, the engineering of growth factors with super-affinity to ECM proteins proved an enhanced wound healing potential when compared to their wild type counterparts [91,92]. Other growth factors from the EGF, FGF, TGFβ, PDGF and VEGF families and their receptors have all been reported to influence wound healing and participate in epidermal and mesenchymal regeneration, as well as in angiogenesis [29,93]. Furthermore, PDGF-BB, FGF, EGF and TGFβ have been previously reported as interesting candidates for the stimulation of amnion-derived mesenchymal stromal cells [29].

Future experiments could characterize the specific cell types present in the amnion. These studies could then precisely describe the local signals taking place in the different areas of the tissue and potentially be used for directing a more specific tissue response. Understanding the localized cellular and ECM crosstalk will enable us to broaden our understanding of the basic mechanisms that drive FM biology, rupture and recovery and is key to the development of biomaterials that will promote the desired tissue response [94]. Restoring FM integrity after an intervention could help in the development of a healthy fetus and newborn and would be a stepping-stone towards solving an unmet clinical need.

CRediT authorship contribution statement

Eva Avilla-Royo: Conceptualization, Investigation, Data curation, Visualization, Writing – original draft, Writing - review & editing. **Katharina Gegenschatz-Schmid:** Methodology, Investigation, Writing – review & editing. **Jonas Grossmann:** Data curation, Software, Validation, Formal analysis, Writing – review & editing. **Tobias Kockmann:** Methodology, Validation, Writing – review & editing. **Roland Zimmermann:** Funding acquisition. **Jess Gerrit Snedeker:** Supervision, Writing - review & editing. **Nicole Ochsenbein-Kölble:** Conceptualization, Resources, Supervision, Writing - review & editing. **Martin Ehrbar:** Conceptualization, Supervision, Funding acquisition, Project administration, Writing - review & editing.

DECLARATION OF COMPETING INTEREST

Acknowledgements

throughout the project and for the revisions of the manuscript and Esther Kleiner (University Hospital Zurich) for her help in sample collection and for technical assistance in histological analysis. We would also like to thank Dr. Unai Silván (Laboratory for Orthopedic Biomechanics, ETH Zurich) for reviewing this manuscript. This work has been supported by the SNSF Grant Nr. 310030_169808/1.

Data availability

The raw and processed MS/MS data from blanks, instrument washes and samples required to reproduce these findings have been deposited to the ProteomeXchange Consortium via the PRIDE partner repository [95] with the dataset identifiers PXD019410 and https://doi.org/10.6019/PXD019410.

Appendix A. Supplementary data

Supplementary data to this article can be found online at https://doi.org/10.1016/j.mbplus.2021.100084.

References

[1] Bryant-Greenwood, G.D., (1998). The extracellular matrix of the human fetal membranes: structure and function. *Placenta*, **19** (1), 1–11.

[2] Ilancheran, S., Moodley, Y., Manuelpillai, U., (2009). Human fetal membranes: a source of stem cells for tissue regeneration and repair? *Placenta*, **30** (1), 2–10.

[3] Epstein, F.H., Parry, S., Strauss, J.F., (1998). Premature rupture of the fetal membranes. *New England J. Med.*, **338** (10), 663–670.

[4] Barrett, D.W., John, R.K., Thrasivoulou, C., Mata, A., Deprest, J.A., Becker, D.L., David, A.L., Chowdhury, T.T., (2019). Targeting mechanotransduction mechanisms and tissue weakening signals in the human amniotic membrane. *Sci. Rep.*, **9** (1) https://doi.org/10.1038/s41598-019-42379-4.

[5] Menon, R., Richardson, L.S., (2017). Preterm prelabor rupture of the membranes: a disease of the fetal membranes. *Semin. Perinatol.*, **41** (7), 409–419.

[6] Nunes, V., Cross, J., Speich, J.E., Morgan, D.R., Strauss, J.F., Ramus, R.M., (2016). Fetal membrane imaging and the prediction of preterm birth: a systematic review, current issues, and future directions. *BMC Pregnancy Childbirth*, **16** (1) https://doi.org/10.1186/s12884-016-1176-5.

[7] Liu, L.i., Oza, S., Hogan, D., Chu, Y., Perin, J., Zhu, J., Lawn, J.E., Cousens, S., Mathers, C., Black, R.E., (2016). Global, regional, and national causes of under-5 mortality in 2000–15: an updated systematic analysis with implications for the Sustainable Development Goals. *The Lancet*, **388** (10063), 3027–3035.

[8] March of Dimes, P., Save the children, World Health Organisation (WHO), Born too soon: the global action report on preterm birth. 2012.

[9] Goldenberg, R.L., Culhane, J.F., Iams, J.D., Romero, R., (2008). Epidemiology and causes of preterm birth. *Lancet*, **371** (9606), 75–84.

[10] Beck, V., Lewi, P., Gucciardo, L., Devlieger, R., (2012). Preterm prelabor rupture of membranes and fetal survival after minimally invasive fetal surgery: a systematic review of the literature. *Fetal Diagn. Ther.*, **31** (1), 1–9.

[11] Ruegg, L. et al, (2020). Outcome after fetoscopic laser coagulation in twin-twin transfusion syndrome - is the survival rate of at least one child at 6 months of age dependent on preoperative cervical length and preterm prelabour rupture of fetal membranes? *J Matern Fetal Neonatal Med*, **33** (5), 852–860.

[12] Möhrlen, U., Ochsenbein-Kölble, N., Mazzone, L., Kraehenmann, F., Hüsler, M., Casanova, B., Biro, P., Wille, D., Latal, B., Scheer, I., Bernet, V., Moehrlen, T., Held, L., Flake, A.W., Zimmermann, R., Meuli, M., (2020). Benchmarking against the MOMS Trial: Zurich Results of Open Fetal Surgery for Spina Bifida. *Fetal Diagn. Ther.*, **47** (2), 91–97.

[13] Gratacós, E., Sanin-Blair, J., Lewi, L., Toran, N., Verbist, G., Cabero, L., Deprest, J., (2006). A histological study of fetoscopic membrane defects to document membrane healing. *Placenta*, **27** (4-5), 452–456.

[14] Amberg, B.J., Hodges, R.J., Rodgers, K.A., Crossley, K.J., Hooper, S.B., DeKoninck, P.L.J., (2021). Why do the fetal membranes rupture early after fetoscopy? a review. *Fetal Diagn. Ther.*, **48** (7), 493–503.

[15] Rocha, S.C.M., Baptista, C.J.M., (2015). Biochemical properties of amniotic membrane. In: Mamede, A.C., Botelho, M.F. (Eds.), *Amniotic Membrane,*. Springer Netherlands, Dordrecht, pp. 19–40.

[16] Barrett, D.W., David, A.L., Thrasivoulou, C., Mata, A., Becker, D.L., Engels, A.C., Deprest, J.A., Chowdhury, T. T., (2016). Connexin 43 is overexpressed in human fetal membrane defects after fetoscopic surgery. *Prenat. Diagn.*, **36** (10), 942–952.

[17] Winkler, S.M., Harrison, M.R., Messersmith, P.B., (2019). Biomaterials in fetal surgery. *Biomater. Sci.*, **7** (8), 3092–3109.

[18] Verbruggen, S.W., Oyen, M.L., Phillips, A.T.M., Nowlan, N.C., Sun, K., (2017). Function and failure of the fetal membrane: modelling the mechanics of the chorion and amnion. *PLoS ONE*, **12** (3), e0171588.

[19] Liu, C., Guo, C., Wang, W., Zhu, P., Li, W., Mi, Y., Myatt, L., Sun, K., (2016). Inhibition of lysyl oxidase by cortisol regeneration in human amnion: implications for rupture of fetal membranes. *Endocrinology*, **157** (10), 4055–4065.

[20] Buerzle, W., Haller, C.M., Jabareen, M., Egger, J., Mallik, A.S., Ochsenbein-Koelble, N., Ehrbar, M., Mazza, E., (2013). Multiaxial mechanical behavior of human fetal

membranes and its relationship to microstructure. *Biomech. Model. Mechanobiol.*, **12** (4), 747–762.

[21] Joyce, E.M., Diaz, P., Tamarkin, S., Moore, R., Strohl, A., Stetzer, B., Kumar, D., Sacks, M.S., Moore, J.J., (2016). In-vivo stretch of term human fetal membranes. *Placenta*, **38**, 57–66.

[22] Hynes, R.O., (2009). The extracellular matrix: not just pretty fibrils. *Science*, **326** (5957), 1216–1219.

[23] Berrier, A.L., Yamada, K.M., (2007). Cell-matrix adhesion. *J. Cell. Physiol.*, **213** (3), 565–573.

[24] Discher, D.E., Mooney, D.J., Zandstra, P.W., (2009). Growth factors, matrices, and forces combine and control stem cells. *Science*, **324** (5935), 1673–1677.

[25] Devlieger, R. et al, (2002). Matrix metalloproteinases-2 and -9 and their endogenous tissue inhibitors in tissue remodeling after sealing of the fetal membranes in a sheep model of fetoscopic surgery. *J. Soc. Gynecol. Investig.*, **9** (3), 137–145.

[26] Strauss, J.F., (2013). Extracellular matrix dynamics and fetal membrane rupture. *Reprod Sci*, **20** (2), 140–153.

[27] Weiss, A., Goldman, S., Shalev, E., (2007). The matrix metalloproteinases (MMPS) in the decidua and fetal membranes. *Front Biosci*, **12**, 649–659.

[28] Caley, M.P., Martins, V.L.C., O'Toole, E.A., (2015). Metalloproteinases and wound healing. *Adv. Wound Care*, **4** (4), 225–234.

[29] Kivelio, A., Ochsenbein-Koelble, N., Zimmermann, R., Ehrbar, M., (2015). Engineered cell instructive matrices for fetal membrane healing. *Acta Biomater.*, **15**, 1–10.

[30] Lee, J.Y., Kim, H., Ha, D.-H., Shin, J.C., Kim, A., Ko, H.S., Cho, D.-W., (2018). Amnion-analogous medical device for fetal membrane healing: a preclinical long-term study. *Adv. Healthcare Mater.*, **7** (18), 1800673.

[31] Liekens, D., Lewi, L., Jani, J., Heyns, L., Poliard, E., Verbist, G., Ochsenbein-Kölble, N., Hoylaerts, M., Deprest, J., (2008). Enrichment of collagen plugs with platelets and amniotic fluid cells increases cell proliferation in sealed iatrogenic membrane defects in the foetal rabbit model. *Prenat. Diagn.*, **28** (6), 503–507.

[32] N. Ochsenbein-Kölble, et al., Enhancing sealing of fetal membrane defects using tissue engineered native amniotic scaffolds in the rabbit model. Am. J. Obstetr. Gynecol., 2007. 196(3): p. 263 e1-7.

[33] Mogami, H., Kishore, A.H., Word, R.A., (2018). Collagen type 1 accelerates healing of ruptured fetal membranes. *Sci. Rep.*, **8** (1), 696.

[34] Kivelio, A., Dekoninck, P., Perrini, M., Brubaker, C.E., Messersmith, P.B., Mazza, E., Deprest, J., Zimmermann, R., Ehrbar, M., Ochsenbein-Koelble, N., (2013). Mussel mimetic tissue adhesive for fetal membrane repair: initial in vivo investigation in rabbits. *Eur. J. Obstet. Gynecol. Reprod. Biol.*, **171** (2), 240–245.

[35] McQuilling, J.P., Kammer, M., Kimmerling, K.A., Mowry, K.C., (2019). Characterisation of dehydrated amnion chorion membranes and evaluation of fibroblast and keratinocyte responses in vitro. *Int. Wound J.*, **16** (3), 827–840.

[36] Fenner, B.J., Yusoff, N.Z.B.M., Fuest, M., Zhou, L., Bandeira, F., Cajucom-Uy, H.Y., Tan, H.K., Mehta, J.S., Yam, G.H.F., (2019). A cellular and proteomic approach to assess proteins extracted from cryopreserved human amnion in the cultivation of corneal stromal keratocytes for stromal cell therapy. *Eye Vision*, **6** (1) https://doi.org/10.1186/s40662-019-0155-0.

[37] Bourne, G.L., The microscopic anatomy of the human amnion and chorion. American Journal of Obstetrics and Gynecology, 1960. 79(6): p. 1070–1073.

[38] Park, S.-J., Yoon, W.-G., Song, J.-S., Jung, H.S., Kim, C.J., Oh, S.Y., Yoon, B.H., Jung, G., Kim, H.-J., Nirasawa, T., (2006). Proteome analysis of human amnion and amniotic fluid by two-dimensional electrophoresis and matrix-assisted laser desorption/ionization time-of-flight mass spectrometry. *Proteomics*, **6** (1), 349–363.

[39] Hopkinson, A. et al, (2006). Proteomic analysis of amniotic membrane prepared for human transplantation: Characterization of proteins and clinical implications. *J. Proteome Res.*, **5**, 2226–2235.

[40] Baharvand, H. et al, (2007). Proteomic analysis of epithelium-denuded human amniotic membrane as a limbal stem cell niche. *Mol. Vision*, **13**, 1711–1721.

[41] Aebersold, R., Mann, M., (2016). Mass-spectrometric exploration of proteome structure and function. *Nature*, **537** (7620), 347–355.

[42] Kim, M.-S., Pinto, S.M., Getnet, D., Nirujogi, R.S., Manda, S.S., Chaerkady, R., Madugundu, A.K., Kelkar, D.S., Isserlin, R., Jain, S., Thomas, J.K., Muthusamy, B., Leal-Rojas, P., Kumar, P., Sahasrabuddhe, N.A., Balakrishnan, L., Advani, J., George, B., Renuse, S., Selvan, L.D.N., Patil, A.H., Nanjappa, V., Radhakrishnan, A., Prasad, S., Subbannayya, T., Raju, R., Kumar, M., Sreenivasamurthy, S.K., Marimuthu, A., Sathe, G.J., Chavan, S., Datta, K.K., Subbannayya, Y., Sahu, A., Yelamanchi, S.D., Jayaram, S., Rajagopalan, P., Sharma, J., Murthy, K.R., Syed, N., Goel, R., Khan, A.A., Ahmad, S., Dey, G., Mudgal, K., Chatterjee, A., Huang, T.-C., Zhong, J., Wu, X., Shaw, P.G., Freed, D., Zahari, M.S., Mukherjee, K.K., Shankar, S., Mahadevan, A., Lam, H., Mitchell, C.J., Shankar, S.K., Satishchandra, P., Schroeder, J.T., Sirdeshmukh, R., Maitra, A., Leach, S.D., Drake, C.G., Halushka, M.K., Prasad, T.S.K., Hruban, R.H., Kerr, C.L., Bader, G.D., Iacobuzio-Donahue, C.A., Gowda, H., Pandey, A., (2014). A draft map of the human proteome. *Nature*, **509** (7502), 575–581.

[43] Wiśniewski, J.R., Zougman, A., Nagaraj, N., Mann, M., (2009). Universal sample preparation method for proteome analysis. *Nat. Methods*, **6** (5), 359–362.

[44] Rappsilber, J., Ishihama, Y., Mann, M., (2003). Stop and go extraction tips for matrix-assisted laser desorption/ionization, nanoelectrospray, and LC/MS sample pretreatment in proteomics. *Anal. Chem.*, **75** (3), 663–670.

[45] Mann, K., Edsinger, E., (2014). The Lottia gigantea shell matrix proteome: re-analysis including MaxQuant iBAQ quantitation and phosphoproteome analysis. *Proteome Science*, **12** (1), 28. https://doi.org/10.1186/1477-5956-12-28.

[46] Y. Liao, et al., WebGestalt 2019: gene set analysis toolkit with revamped UIs and APIs. Nucleic Acids Res, 2019. 47 (W1): p. W199-W205.

[47] A. Naba, et al., The matrisome: in silico definition and in vivo characterization by proteomics of normal and tumor extracellular matrices. Mol Cell Proteomics, 2012. 11(4): p. M111 014647.

[48] R.O. Hynes, A. Naba, Overview of the matrisome-an inventory of extracellular matrix constituents and functions. Cold Spring Harb Perspect Biol, 2012. 4(1): p. a004903.

[49] Hulsen, T., de Vlieg, J., Alkema, W., (2008). BioVenn – a web application for the comparison and visualization of

biological lists using area-proportional Venn diagrams. *BMC Genomics*, **9**, 488.

[50] Y. Liao, G.K. Smyth, W. Shi, The R package Rsubread is easier, faster, cheaper and better for alignment and quantification of RNA sequencing reads. Nucleic Acids Res, 2019. 47(8): p. e47.

[51] Wolski, W., Grossman, J., (2018). and C. Panse, SRMService - R-Package to Report Quantitative Mass Spectrometry Data.

[52] G.K. Smyth, Linear models and empirical bayes methods for assessing differential expression in microarray experiments. Stat Appl. Genet. Mol. Biol., 2004. 3: p. Article3.

[53] M.E. Ritchie, et al., Limma powers differential expression analyses for RNA-sequencing and microarray studies. Nucleic Acids Res, 2015. 43(7): p. e47.

[54] G.R. Warrnes, et al., gplots: Various R Programming Tools for Plotting Data. R package version 2, 2019.

[55] Schindelin, J., Arganda-Carreras, I., Frise, E., Kaynig, V., Longair, M., Pietzsch, T., Preibisch, S., Rueden, C., Saalfeld, S., Schmid, B., Tinevez, J.-Y., White, D.J., Hartenstein, V., Eliceiri, K., Tomancak, P., Cardona, A., (2012). Fiji: an open-source platform for biological-image analysis. *Nat. Methods*, **9** (7), 676–682.

[56] Schneider, C.A., Rasband, W.S., Eliceiri, K.W., (2012). NIH Image to ImageJ: 25 years of image analysis. *Nat. Methods*, **9** (7), 671–675.

[57] Ludwig, K.R., Schroll, M.M., Hummon, A.B., (2018). Comparison of in-solution, FASP, and S-Trap based digestion methods for bottom-up proteomic studies. *J. Proteome Res.*, **17** (7), 2480–2490.

[58] Cox, J., Mann, M., (2008). MaxQuant enables high peptide identification rates, individualized p.p.b.-range mass accuracies and proteome-wide protein quantification. *Nat. Biotechnol.*, **26** (12), 1367–1372.

[59] Kumar, D. et al, (2006). Proinflammatory cytokines found in amniotic fluid induce collagen remodeling, apoptosis, and biophysical weakening of cultured human fetal membranes. *Biol. Reprod.*, **74** (1), 29–34.

[60] Naba, A., Clauser, K.R., Ding, H., Whittaker, C.A., Carr, S.A., Hynes, R.O., (2016). The extracellular matrix: Tools and insights for the "omics" era. *Matrix Biol.*, **49**, 10–24.

[61] Bekker-Jensen, D.B., Kelstrup, C.D., Batth, T.S., Larsen, S.C., Haldrup, C., Bramsen, J.B., Sørensen, K.D., Høyer, Søren, Ørntoft, T.F., Andersen, C.L., Nielsen, M.L., Olsen, J.V., (2017). An optimized shotgun strategy for the rapid generation of comprehensive human proteomes. *Cell Systems*, **4** (6), 587–599.e4.

[62] Wang, Y., Yang, F., Gritsenko, M.A., Wang, Y., Clauss, T., Liu, T., Shen, Y., Monroe, M.E., Lopez-Ferrer, D., Reno, T., Moore, R.J., Klemke, R.L., Camp, D.G., Smith, R.D., (2011). Reversed-phase chromatography with multiple fraction concatenation strategy for proteome profiling of human MCF10A cells. *Proteomics*, **11** (10), 2019–2026.

[63] Pereyra, S., Sosa, C., Bertoni, B., Sapiro, R., (2019). Transcriptomic analysis of fetal membranes reveals pathways involved in preterm birth. *BMC Med. Genomics*, **12** (1), 53.

[64] Ween, M.P., Oehler, M.K., Ricciardelli, C., (2012). Transforming growth Factor-Beta-Induced Protein (TGFBI)/(betaig-H3): a matrix protein with dual functions in ovarian cancer. *Int. J. Mol. Sci.*, **13** (8), 10461–10477.

[65] Chakravarti, S., (2002). Functions of lumican and fibromodulin: lessons from knockout mice. *Glycoconj. J.*, **19** (4/5), 287–293.

[66] Reed, C.C., Iozzo, R.V., (2002). The role of decorin in collagen fibrillogenesis and skin homeostasis. *Glycoconj. J.*, **19** (4/5), 249–255.

[67] Okamoto, O., Fujiwara, S., (2006). Dermatopontin, a novel player in the biology of the extracellular matrix. *Connect. Tissue Res.*, **47** (4), 177–189.

[68] Zhu, S. et al, (2021). Molecular structure and function of microfibrillar-associated proteins in skeletal and metabolic disorders and cancers. *J. Cell. Physiol.*, **236** (1), 41–48.

[69] Lamandé, S.R., Bateman, J.F., (2018). Collagen VI disorders: insights on form and function in the extracellular matrix and beyond. *Matrix Biol.*, **71-72**, 348–367.

[70] Thomson, J., Singh, M., Eckersley, A., Cain, S.A., Sherratt, M.J., Baldock, C., (2019). Fibrillin microfibrils and elastic fibre proteins: Functional interactions and extracellular regulation of growth factors. *Semin. Cell Dev. Biol.*, **89**, 109–117.

[71] D. Szklarczyk, et al., STRING v11: protein-protein association networks with increased coverage, supporting functional discovery in genome-wide experimental datasets. Nucleic Acids Res, 2019. 47(D1): p. D607-D613.

[72] Meinert, M., Eriksen, G.V., Petersen, A.C., Helmig, R.B., Laurent, C., Uldbjerg, N., Malmström, A., (2001). Proteoglycans and hyaluronan in human fetal membranes. *Am. J. Obsterics Gynecol.*, **184** (4), 679–685.

[73] M.L. Calmus, et al., A mouse model of spontaneous preterm birth based on the genetic ablation of biglycan and decorin. Reproduction, 2011. 142(1): p. 183–194.

[74] Wu, Z., Horgan, C.E., Carr, O., Owens, R.T., Iozzo, R.V., Lechner, B.E., (2014). Biglycan and decorin differentially regulate signaling in the fetal membranes. *Matrix Biol.*, **35**, 266–275.

[75] Kalamajski, S., Oldberg, Å., (2010). The role of small leucine-rich proteoglycans in collagen fibrillogenesis. *Matrix Biol.*, **29** (4), 248–253.

[76] Yeh, L.-K., Chen, W.-L., Li, W., Espana, E.M., Ouyang, J., Kawakita, T., Kao, W.-Y., Tseng, S.C.G., Liu, C.-Y., (2005). Soluble lumican glycoprotein purified from human amniotic membrane promotes corneal epithelial wound healing. *Invest. Ophthalmol. Vis. Sci.*, **46** (2), 479–486.

[77] Stm, M., Liu, Y., Gibb, W., (1996). Distribution of annexin I and II in term human fetal membranes, decidua and placenta. *Placenta*, **17**, 181–184.

[78] Hitchcock, J.K., Katz, A.A., Schäfer, G., (2014). Dynamic reciprocity: the role of annexin A2 in tissue integrity. *J. Cell Commun. Signaling*, **8** (2), 125–133.

[79] Ryan, D.G., Taliana, L., Sun, L., Wei, Z.-G., Masur, S.K., Lavker, R.M., (2003). Involvement of S100A4 in stromal fibroblasts of the regenerating cornea. *Invest. Ophthalmol. Vis. Sci.*, **44** (10), 4255. https://doi.org/10.1167/iovs.03-0578.

[80] Gobbetti, T., Cooray, S.N., (2016). Annexin A1 and resolution of inflammation: tissue repairing properties and signalling signature. *Biol. Chem.*, **397** (10), 981–993.

[81] U. Consortium, UniProt: a worldwide hub of protein knowledge. Nucleic Acids Res, 2019. 47(D1): p. D506-D515.

[82] S.C. Riley, et al., Secretion of tissue inhibitors of matrix metalloproteinases by human fetal membranes, decidua

and placenta at parturition. J. Endocrinol., 1999. 162: p. 351–359.

[83] Lucero, H.A., Kagan, H.M., (2006). Lysyl oxidase: an oxidative enzyme and effector of cell function. *Cell. Mol. Life Sci*., **63** (19-20), 2304–2316.

[84] D. Hieber, et al., Detection of Elastin in the Human Fetal Membranes: Proposed Molecular Basis for Elasticity. 1997: p. 301–312.

[85] Dakin, S.G., Smith, R.K.W., Heinegård, D., Önnerfjord, P., Khabut, A., Dudhia, J., (2014). Proteomic analysis of tendon extracellular matrix reveals disease stage-specific fragmentation and differential cleavage of COMP (cartilage oligomeric matrix protein). *J. Biol. Chem*., **289** (8), 4919–4927.

[86] Schmelzer, C.E.H., Hedtke, T., Heinz, A., (2020). Unique molecular networks: formation and role of elastin cross-links. *IUBMB Life*, **72** (5), 842–854.

[87] Li, H., Fredriksson, L., Li, X., Eriksson, U., (2003). PDGF-D is a potent transforming and angiogenic growth factor. *Oncogene*, **22** (10), 1501–1510.

[88] Papageorgiou, P. et al, (2019). Expanded skeletal stem and progenitor cells promote and participate in induced bone regeneration at subcritical BMP-2 dose. *Biomaterials*, **217**, 119278

[89] Purcell, B.P., Lobb, D., Charati, M.B., Dorsey, S.M., Wade, R.J., Zellars, K.N., Doviak, H., Pettaway, S., Logdon, C.B., Shuman, J.A., Freels, P.D., Gorman III, J. H., Gorman, R.C., Spinale, F.G., Burdick, J.A., (2014). Injectable and bioresponsive hydrogels for on-demand matrix metalloproteinase inhibition. *Nat. Mater*., **13** (6), 653–661.

[90] Qu, F., Holloway, J.L., Esterhai, J.L., Burdick, J.A., Mauck, R.L., (2017). Programmed biomolecule delivery to enable and direct cell migration for connective tissue repair. *Nat. Commun*., **8** (1), 1780.

[91] Martino, M.M., Briquez, P.S., Guc, E., Tortelli, F., Kilarski, W.W., Metzger, S., Rice, J.J., Kuhn, G.A., Muller, R., Swartz, M.A., Hubbell, J.A., (2014). Growth factors engineered for super-affinity to the extracellular matrix enhance tissue healing. *Science*, **343** (6173), 885–888.

[92] Mochizuki, M., Güç, E., Park, A.J., Julier, Z., Briquez, P.S., Kuhn, G.A., Müller, R., Swartz, M.A., Hubbell, J.A., Martino, M.M., (2020). Growth factors with enhanced syndecan binding generate tonic signalling and promote tissue healing. *Nature Biomed. Eng*., **4** (4), 463–475.

[93] Arwert, E.N., Hoste, E., Watt, F.M., (2012). Epithelial stem cells, wound healing and cancer. *Nat. Rev. Cancer*, **12** (3), 170–180.

[94] Blache, U., Stevens, M.M., Gentleman, E., (2020). Harnessing the secreted extracellular matrix to engineer tissues. *Nat. Biomed. Eng*., **4** (4), 357–363.

[95] Perez-Riverol, Y., Csordas, A., Bai, J., Bernal-Llinares, M., Hewapathirana, S., Kundu, D.J., Inuganti, A., ... Jarnuczak, A.F., Ternent, T., Brazma, A., Vizcaíno, J.A., (2019). The PRIDE database and related tools and resources in 2019: improving support for quantification data. *Nucleic Acids Res*, **47** (D1), D442–D450. https://doi.org/10.1093/nar/gky1106.